



## A Mathematical Model for Quorum Sensing in *Pseudomonas aeruginosa*

JACK D. DOCKERY\*

Department of Mathematics,  
Montana State University,  
Bozeman,  
MT 59718, U.S.A.

*E-mail:* umsfjdoc@math.montana.edu

JAMES P. KEENER

Department of Mathematics,  
University of Utah,  
Salt Lake City,  
UT 84112, U.S.A.

*E-mail:* keener@math.utah.edu

The bacteria *Pseudomonas aeruginosa* use the size and density of their colonies to regulate the production of a large variety of substances, including toxins. This phenomenon, called quorum sensing, apparently enables colonies to grow to sufficient size undetected by the immune system of the host organism.

In this paper, we present a mathematical model of quorum sensing in *P. aeruginosa* that is based on the known biochemistry of regulation of the autoinducer that is crucial to this signalling mechanism. Using this model we show that quorum sensing works because of a biochemical switch between two stable steady solutions, one with low levels of autoinducer and one with high levels of autoinducer.

© 2000 Society for Mathematical Biology

### 1. INTRODUCTION

The bacterium *Pseudomonas aeruginosa* is an increasingly prevalent human pathogen, responsible for 12% of hospital-acquired urinary tract infections, 10% of blood stream infections, and 8% of surgical wound infections. It is also one of the most common and lethal pathogens responsible for ventilator-associated pneumonia in intubated patients, with directly attributable deaths reaching 38%. Cystic fibrosis patients are characteristically susceptible to chronic infection by *P. aeruginosa*, which is responsible for high rates of illness and death in this population (Van Delden and Iglewski, 1998).

The ability of *P. aeruginosa* to invade a potential host relies largely on its ability to control many of its virulence factors by a mechanism that monitors cell density

Author:  
Van Delden and Iglewski  
(1998) OK? or Van  
Delden *et al.* please check

\*Author to whom correspondence should be addressed.

and allows communication between bacteria. That is, isolated production of extracellular virulence factors by a small number of bacteria would probably lead to an efficient host response neutralizing these factors. However, the typical behavior is for virulence factors to be expressed by an entire colony only after the colony has achieved a certain size or density. In this way, cells excrete extracellular virulence factors only when they can be produced at high enough levels to overcome host defenses.

Another feature of persistent *P. aeruginosa* infections in cystic fibrosis patients is that when cell densities are high enough, the population as a whole begins to produce copious amounts of exopolysaccharide alginate (Govan and Deretic, 1996). It is thought that these bacteria grow inside a biofilm [defined as micro-colonies surrounded by an exopolysaccharide, see Characklis and Marshall (1990)] as a survival strategy since the surrounding polymer matrix protects bacteria. *P. aeruginosa* growing in an alginate 'slime matrix' are resistant to antibiotics and disinfectants (Govan and Deretic, 1996).

Recently, a cell-to-cell signaling system has been shown to be involved in the differentiation of *P. aeruginosa* biofilms (Davies *et al.*, 1998). A mutant defective in the production of a certain signaling molecule formed an abnormal biofilm that in contrast to the wild type biofilm was sensitive to low concentrations of the detergent sodium dodecyl sulfate (SDS). Furthermore, the addition of the signaling molecule to the batch culture medium restored production of a slimy biofilm that was SDS resistant (Davies *et al.*, 1998).

The ability of cells to sense their own cell density, to communicate with each other and to behave as a population instead of individually is called quorum sensing. Quorum sensing is known to occur in a growing number of examples, including sporulation and fruiting body formation by *Myxococcus xanthus* and antibiotic production by several species of *Streptomyces*. Perhaps the best characterized example is in the autoinduction of luminescence in the symbiotic marine bacterium *Vibrio fischeri*, which colonizes the light organs of certain marine fishes and squids (Fuqua *et al.*, 1996).

In all of these examples the fundamental mechanism of quorum sensing is the same, although the biochemical details are surprisingly different. These cell-to-cell signaling systems are all composed of a small molecule, called an autoinducer, which is synthesized by an autoinducer synthase, and a transcriptional activator protein. The production of the autoinducer is regulated by a specific R-protein. The R-protein by itself is not active without the corresponding autoinducer, but the R-protein/autoinducer complex binds to specific DNA sequences upstream of the target genes, enhancing their transcription. Thus, at low cell density, the autoinducer is synthesized at basal levels and diffuses into the surrounding medium, where it is diluted. With increasing cell density, however, the intracellular concentration of the autoinducer increases until it reaches a threshold concentration beyond which it is produced autocatalytically, resulting in a dramatic increase of product concentrations. The autoinducer, therefore, allows the bacteria to communicate with each

Author:  
Govan and Deretic (1996)  
OK?  
Author:  
Characklis and Marshall  
(1990) OK?

other, to sense their own density, and together with a transcriptional activator to express specific genes as a population rather than individually.

Quorum sensing is an unusual signaling mechanism for several reasons. First, there are no membrane surface receptors for the signaling molecule, and since the autoinducer is produced on the interior of the cell, the extracellular concentration of autoinducer is generally smaller than the intracellular concentration. One might therefore question how the autoinducer can act as a signal.

The purpose of this paper is to develop and study mathematical models of quorum sensing, in order to obtain a deeper understanding of how and when this mechanism works. We focus on the specific system of *P. aeruginosa* although the mathematical principles are the same in other systems. Our emphasis here is on the biochemical mechanism underlying quorum sensing. In a related study, James *et al.* (2000) found a simple mathematical model appropriate to *V. fischeri* that had multiple stable steady states and was controlled by extracellular autoinducer. By contrast, in Ward *et al.* (2000), a population dynamics approach was taken for *V. fischeri*, and switching behavior in which there was cell differentiation was found as the colony grew in size. The models in both of these studies were systems of three first-order, nonlinear, ordinary differential equations. In what follows, we examine models involving both ordinary and partial differential equations.

## 2. THE MODEL

The quorum-sensing system of *P. aeruginosa* is unusual because it has two somewhat redundant regulatory systems. The first system described in *P. aeruginosa* was shown to regulate expression of the elastase LasB and was therefore named the *las* system. The two enzymes, LasB elastase and LasA elastase, are responsible for elastolytic activity which destroys elastin-containing human lung tissue and causes pulmonary hemorrhages associated with *P. aeruginosa* infections. The *las* system is composed of *lasI*, the autoinducer synthase gene responsible for synthesis of the autoinducer 3-oxo-C12-HSL, and the *lasR* gene that codes for transcriptional activator protein. The LasR/3-oxo-C12-HSL dimer, which is the activated form of LasR, activates a variety of genes, but preferentially promotes *lasI* activity. The *las* system is positively controlled by both GacA and Vfr, which are needed for transcription of *lasR*. The transcription of *lasI* is also repressed by the inhibitor RsaL.

The second quorum-sensing system in *P. aeruginosa* is named the *rhl* system because of its ability to control the production of rhamnolipid. Rhamnolipid has a detergent-like structure and is responsible for the degradation of lung surfactant and inhibits the mucociliary transport and ciliary function of human respiratory epithelium. This system is composed of *rhlI*, the synthase gene for the autoinducer C4-HSL, and the *rhlR* gene encoding a transcriptional activator protein. A diagram depicting these two systems is shown in Fig. 1 (Van Delden and Iglewski, 1998).

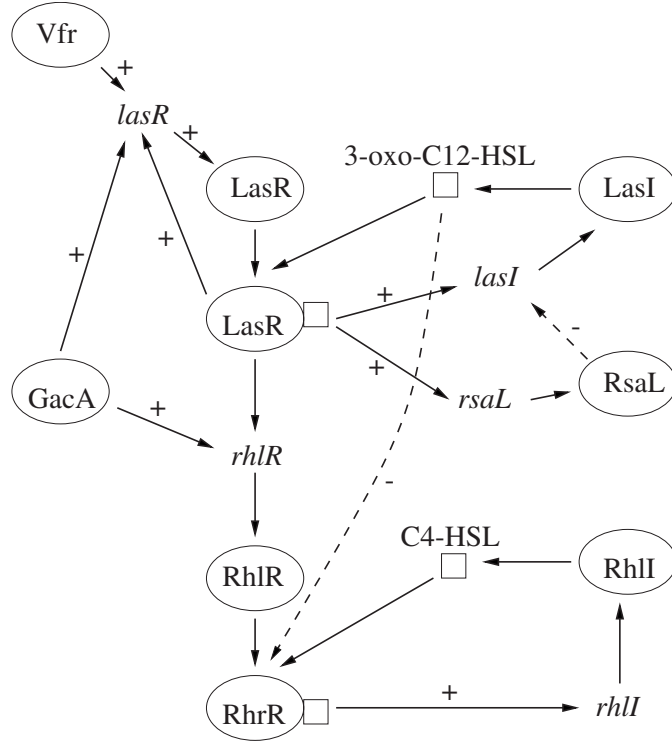


Figure 1. Schematic diagram showing the gene regulation for the *las* and *rhl* systems in *P. aeruginosa*.

The first step in our analysis is to find equations describing the kinetics of this system. For simplicity, we consider only the *las* system. We introduce variables for all the concentrations (shown in Table 1). We assume that the dimer  $P$  is formed via the law of mass action at rate  $k_{RA}$  and degraded at rate  $k_P$ ,

$$\frac{dP}{dt} = k_{RA}RA - k_P P. \quad (1)$$

The enzyme LasR is used in the production of  $P$  and naturally degrades at rate  $k_R$ , and is produced by the degradation of  $P$ , and by *lasR* mRNA at rate  $k_1$ ,

$$\frac{dR}{dt} = -k_{RA}RA + k_P P - k_R R + k_1 r. \quad (2)$$

Similarly, the autoinducer is used in the production of  $P$  and naturally degrades at rate  $k_A$ , and is produced by the degradation of  $P$ , and by the *lasI* enzyme at rate  $k_2$ ,

$$\frac{dA}{dt} = -k_{RA}RA + k_P P + k_2 L - k_A A. \quad (3)$$

Table 1. Variables used to identify concentrations.

Variable	Concentration
$R$	LasR
$A$	3-oxo-C12-HSL
$P$	LasR/3-oxo-C12-HSL
$L$	LasI
$S$	RsaL
$r$	lasR mRNA
$l$	lasI mRNA
$s$	rsaL mRNA

The enzyme LasI is produced by lasI mRNA at rate  $k_3$  and degrades at rate  $k_L$ ,

$$\frac{dL}{dt} = k_3l - k_L L. \quad (4)$$

The inhibitor RsaL is produced by rsaL mRNA at rate  $k_4$  and degrades at rate  $k_S$ ,

$$\frac{dS}{dt} = k_4s - k_S S. \quad (5)$$

All messenger RNAs are produced by DNA at rates that are Michaelis–Menten in type. Thus, for example, the inhibitor rsaL mRNA is produced at a Michaelis–Menten rate depending on  $P$ , and degrades at some natural rate  $k_s$ ,

$$\frac{ds}{dt} = V_s \frac{P}{K_s + P} - k_s s, \quad (6)$$

and similarly, lasR mRNA is produced at a Michaelis–Menten rate depending on  $P$ , and degrades at some natural rate  $k_r$ . We also assume that lasR mRNA is produced at some basal rate  $r_0$ .

$$\frac{dr}{dt} = V_r \frac{P}{K_r + P} - k_r r + r_0. \quad (7)$$

Finally, the production of lasI mRNA is activated by  $P$  and inactivated by  $S$ , degrades at rate  $l_l$ , and is produced at some basal rate  $l_0$ ,

$$\frac{dl}{dt} = V_l \frac{P}{K_l + P} \frac{1}{K_S + S} - k_l l + l_0. \quad (8)$$

We would like to simplify this system by taking into account that some reactions are fast compared to others. The difficulty here is that the rate constants in the model are not known. There is evidence that many proteins are more stable than the mRNA that code for them [see, for example, Anderson *et al.* (1998), Chalfie *et al.* (1998) and Ehrenberg and Sverredal (1995)]. If this is the case here, then LasR

Author:  
"Ehrenberg and  
Sverredal" (1995) OK?

mRNA and lasI mRNA are much shorter lived than LasR and LasL, respectively, so that  $k_r$  and  $k_l$  are much larger than  $k_L$  and  $k_R$ . With this assumption, we take  $l$  and  $r$  to be in quasi-steady state, so that

$$k_l l = V_l \frac{P}{K_l + P} \frac{1}{K_S + S} + l_0, \quad k_r r = V_r \frac{P}{K_r + P} + r_0. \quad (9)$$

The variable  $L$  can be understood as a first-order linear filter, so that  $L$  tracks  $l$  with some delay. The simplest approximation to this behavior is to ignore the delay and take

$$k_3 l = k_L L. \quad (10)$$

The quantity  $S$  inhibits the production of  $l$ , but it seems not to have much effect on quorum-sensing behavior. We ignore this variable by eliminating it from the production term in equation (8).

With these simplifications, the governing system of equations becomes

$$\frac{dP}{dt} = k_{RA} RA - k_P P, \quad (11)$$

$$\frac{dR}{dt} = -k_{RA} RA + k_P P - k_R R + V_R \frac{P}{K_R + P} + R_0, \quad (12)$$

$$\frac{dA}{dt} = -k_{RA} RA + k_P P + V_A \frac{P}{K_L + P} + A_0 - k_A A, \quad (13)$$

(with redefined parameters, of course). Finally, since the production of  $A$  and  $R$  involves transcription of mRNA, it is probably slow compared to the binding and unbinding of  $R$  and  $A$  to form complex  $P$ . Thus, we assume that  $P$  is in quasi-steady state so that

$$k_P P = k_{RA} RA \quad (14)$$

and the governing equations become

$$\frac{dR}{dt} = -k_R R + V_R \frac{P}{K_R + P} + R_0, \quad (15)$$

$$\frac{dA}{dt} = V_A \frac{P}{K_L + P} + A_0 - k_A A, \quad (16)$$

$$P = \frac{k_{RA}}{k_P} RA. \quad (17)$$

Next, we need to determine how the density of organisms controls the activity of this network. We assume that autoinducer  $A$  diffuses across the cell membrane, and that the local density (volume fraction) of cells is  $\rho$ . Then by assumption, the local volume fraction of extracellular space is  $1 - \rho$ .

Author:  
Equation number (14)  
avoided after  
equation (13) OK? (please  
check hard copy)

The extracellular autoinducer is assumed to diffuse freely across the cell membrane, with conductance  $\delta$ , and naturally degrades at rate  $k_E$ . If we suppose that the density of cells is uniform and the extracellular space is well mixed, then the concentration of autoinducer in the extracellular space, denoted  $E$ , is governed by the equation

$$(1 - \rho) \left( \frac{dE}{dt} + k_E E \right) = \delta(A - E). \quad (18)$$

Here the factor  $1 - \rho$  must be included to scale for the difference between concentration in the extracellular space and concentration viewed as amount per unit total volume. Similarly, the governing equation for intracellular autoinducer  $A$  must be modified to account for diffusion across the cell membrane, yielding

$$\rho \left( \frac{dA}{dt} - V_A \frac{P}{K_L + P} - A_0 + k_A A \right) = -\delta(A - E). \quad (19)$$

There is some evidence that the transport of the autoinducer may involve both passive diffusion and a cotransport mechanism (Pearson *et al.*, 1999). For this model we assume that diffusion alone acts to transport the autoinducer [as is apparently correct for the *rhl* system (Pearson *et al.*, 1999)]. The inclusion here of an additional cotransport mechanism is possible but seems not to be a crucial ingredient.

It is now fairly easy to see that this system of equations exhibits quorum sensing. One way to see this is to take  $E$  to be in quasi-steady state. This is probably not a good assumption since  $A$  and  $E$  are the same chemical and so probably degrade at about the same rates inside and outside the cell. However, this assumption allows us to study this system in the phase plane. The behavior is not changed if a three-variable system is used, but the analysis of the three-variable systems is substantially more complicated with little increase in insight.

The resulting system is (with redefined parameters)

$$\frac{dR}{dt} = V_R \frac{P}{K_R + P} - k_R R + R_0, \quad (20)$$

$$\frac{dA}{dt} = V_A \frac{P}{K_A + P} + A_0 - d(\rho)A, \quad (21)$$

where  $P = \frac{k_{RA}RA}{k_P}$  and  $d(\rho) = k_A + \frac{\delta}{\rho} \left( \frac{k_E(1-\rho)}{\delta + k_E(1-\rho)} \right)$ .

Quorum sensing works because of the  $\rho$  dependence of  $d(\rho)$ . In particular, when  $\rho$  is small,  $d(\rho)$ , the decay rate for  $A$ , is large, while when  $\rho$  is close to one,  $d(\rho)$  is small. This has the feature of modifying the  $A$  nullcline in an important way. The nullclines for the system (20), (21) are shown in Fig. 2. Here it is readily seen that for small values of  $\rho$  and for large values of  $\rho$  there is a unique steady-state solution in the positive  $R$ - $A$  quadrant. For small values of  $\rho$  the steady-state values

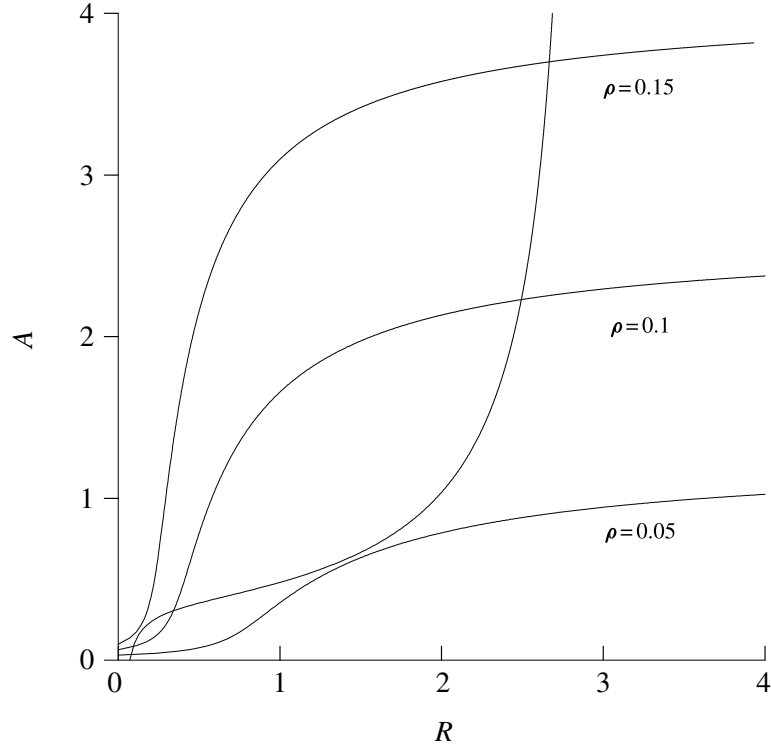


Figure 2. Nullclines  $\frac{dR}{dt} = -k_R R + \frac{V_R R A}{K_R + R A} + R_0 = 0$  and  $\frac{dA}{dt} = \frac{V_A R A}{K_A + R A} + A_0 - d(\rho)A = 0$  with three different values of  $\rho$ , shown for parameter values  $V_R = 2.0$ ,  $V_A = 2.0$ ,  $K_R = 1.0$ ,  $K_A = 1.0$ ,  $R_0 = 0.05$ ,  $A_0 = 0.05$ ,  $\delta = 0.2$ ,  $k_E = 0.1$ ,  $k_R = 0.7$ , and  $k_A = 0.02$ .

of  $R$  and  $A$  are small, while for large values of  $\rho$  the steady state-values of  $R$  and  $A$  are large.

For intermediate values of  $\rho$ , there are three steady solutions in the positive quadrant. The small and large values are stable steady solutions while the intermediate solution is unstable, a saddle point.

The parameter  $\rho$  provides a switch between the two stable steady solutions. For small values of  $\rho$ , there is a unique stable steady state with small values of  $R$  and  $A$ . As  $\rho$  increases, two more solutions appear (a saddle node bifurcation), and as  $\rho$  increases yet further, the small solution disappears (another saddle node) leaving a unique solution, thus initiating a ‘switch’.

It is easy to arrange parameter values that have this switching behavior, and the switch can be adjusted to occur at any desired density level.

An even simpler model that has the same qualitative behavior (but is not correct from a biochemical perspective) is found by setting  $R = A$  to obtain

$$\frac{dA}{dt} = V_A \frac{A^2}{K_A + A^2} + A_0 - d(\rho)A. \quad (22)$$

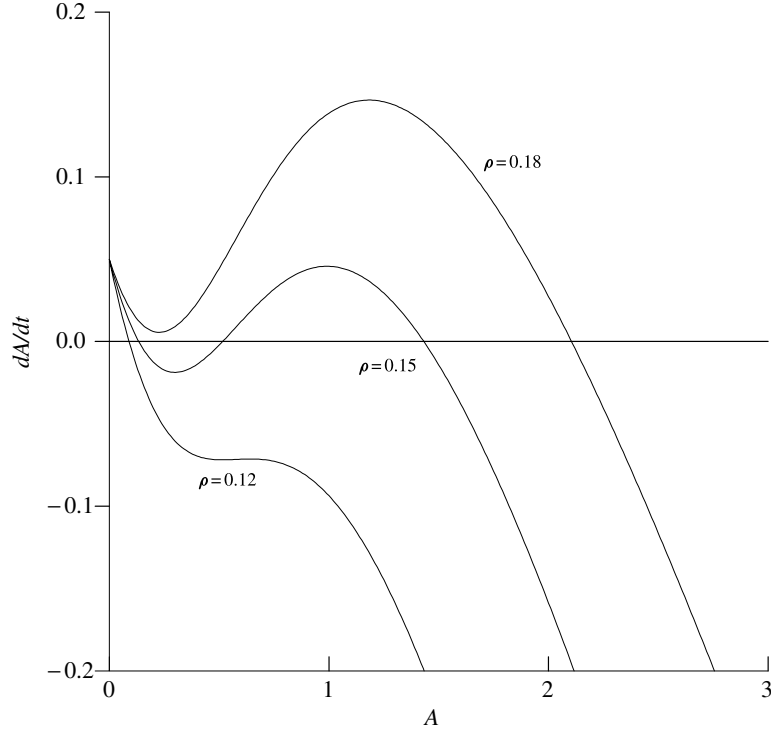


Figure 3. Plot of  $\frac{dA}{dt} = \frac{V_A A^2}{K_A + A^2} + A_0 - d(\rho)A$  as a function of  $A$  for several values of  $\rho$  with parameter values  $V_A = 1.0$ ,  $K_A = 1.0$ ,  $A_0 = 0.05$ ,  $\delta = 0.5$ ,  $k_E = 0.1$ , and  $k_A = 0.02$ .

Here, the curve  $\frac{dA}{dt}$ , shown in Fig. 3, is a monotone increasing function of  $\rho$  and for small and large values of  $\rho$  there is a unique positive steady-state solution. For small values of  $\rho$  the steady-state value of  $A$  is small, while for large values of  $\rho$  the steady-state value of  $A$  is large.

For intermediate values of  $\rho$ , the curve  $\frac{dA}{dt}$  is ‘n-shaped’ and there are three steady positive solutions. The small and large values are stable steady solutions while the intermediate solution is unstable.

The switching behavior is readily observed by varying  $\rho$ . For small values of  $\rho$ , there is a unique stable steady state with a small value of  $A$ . As  $\rho$  increases, two more solutions appear, and as  $\rho$  increases yet further, the small solution disappears leaving a unique solution, thus initiating a ‘switch’.

We can now give a verbal explanation of how quorum sensing works. The quantity  $A$ , the autoinducer, is produced by cells at some nominal rate. However, the cell must dump its production of  $A$  or else the autocatalytic reaction would turn on. As the density of cells increases, the dumping process becomes less effective, and so the autocatalytic reaction is turned on. In other words, quorum sensing takes place because the ‘drain’ for  $A$  backs up. Note that the external concentration of

$A$  is always smaller than the internal concentration of  $A$ . Thus,  $A$  is not actually a signaling chemical, and there is no necessity for surface receptors for  $A$ , and there is no need to develop high concentrations of autoinducer in the extracellular space.

### 3. A PDE MODEL

While the above model shows the desired behavior in a homogeneous environment, such as a chemostat, a more realistic model would take into account the possibility of inhomogeneous distributions of the autoinducer in the extracellular space, while the cells themselves remain relatively motionless.

We suppose there is a uniform layer of cells of thickness  $L$  and fixed volume fraction  $\rho$  which are attached to a substratum in an aqueous bath. As above, the cells produce the autoinducer with concentration  $A$  which has extracellular concentration  $E$ ,

$$\frac{dA}{dt} = F(A) + \frac{\delta}{\rho}(E - A), \quad (23)$$

$$\frac{\partial E}{\partial t} = \frac{\partial^2 E}{\partial x^2} + \frac{\delta}{1 - \rho}(A - E) - k_E E. \quad (24)$$

The factor  $\rho$  in equation (23) and the factor  $1 - \rho$  in (24) are necessary to account for the differences in volume fraction between intracellular and extracellular space. We assume that the cells occupy the one-dimensional region  $0 < x < L$ . At the boundary of the cellular domain,  $x = L$ , we assume that there is mass transfer into the bulk fluid. We model this simply by assuming the Robin boundary condition

$$E_x(L, t) + \alpha E(L, t) = 0 \quad (25)$$

where  $\alpha$  is a positive parameter. At the substratum we impose the Neumann boundary condition

$$E_x(0, t) = 0. \quad (26)$$

The goal of this section is to find the steady-state solutions of this pde, i.e.,

$$E_{xx} + \frac{\delta}{1 - \rho}(A - E) - k_E E = 0, \quad \text{with} \quad F(A) + \frac{\delta}{\rho}(E - A) = 0 \quad (27)$$

on  $0 < x < L$  with  $E_x(0) = 0$  and  $E_x(L) + \alpha E(L) = 0$ .

The analysis of this equation is accomplished in the phase plane. First, we must determine the nature of the solutions of the equation

$$F(A) + \frac{\delta}{\rho}(E - A) = 0. \quad (28)$$

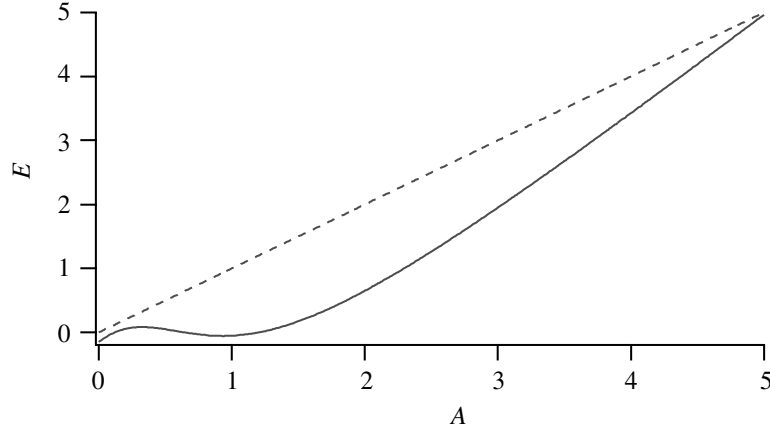


Figure 4. Plot of the function  $E(A) = A - \frac{\delta}{8}F(A)$  for  $K_A = 1.0$ ,  $V_A = 1.0$ ,  $A_0 = 0.05$ ,  $\delta = 0.1$ ,  $\rho = 0.3$ , and  $k_A = 0.2$ .

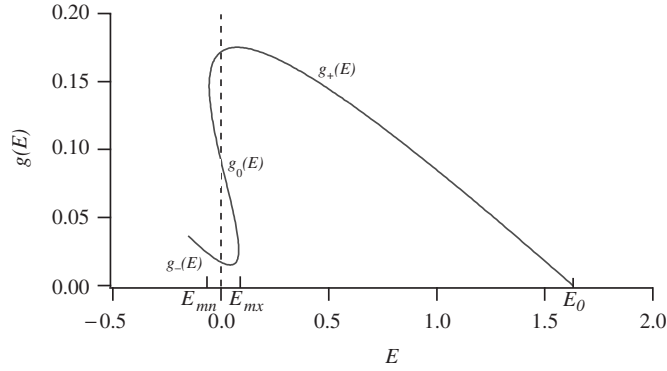


Figure 5. Plot of the 'function'  $g(E) = \frac{\delta}{1-\rho}(A^{-1}(E) - E) - k_E E$  for  $K_A = 1.0$ ,  $V_A = 1.0$ ,  $A_0 = 0.05$ ,  $\delta = 0.1$ ,  $\rho = 0.3$ ,  $k_A = 0.2$ , and  $k_E = 0.1$ .

We begin by stating general assumptions for the function  $F(A)$ , namely that it is 'n-shaped' and strictly positive on the interval  $0 \leq A < A^*$ , and that  $F(A^*) = 0$ . A specific example of the function  $F(A)$  is

$$F(A) = \frac{V_A A^2}{K_A + A^2} - k_A A + A_0. \quad (29)$$

This function is 'n-shaped' if  $k_A < \frac{3V_A}{8} \sqrt{\frac{3}{K_A}}$  and has only one zero if  $A_0$  is sufficiently large.

It is easy to determine  $E$  as a function of  $A$  from (28) (shown in Fig. 4). We further assume that  $\frac{\delta}{8}$  is sufficiently large so that the function  $E(A) = A - \frac{\delta}{8}F(A)$  is an 'n-shaped' function. For the function (29), this occurs whenever  $\frac{\delta}{\rho} < \frac{3V_A}{8} \sqrt{\frac{3}{K_A}} - k_A$ . Since  $E(A) = A - \frac{\delta}{8}F(A)$  is 'n-shaped', there are values  $A_{mx}$  and  $A_{mn}$ , with

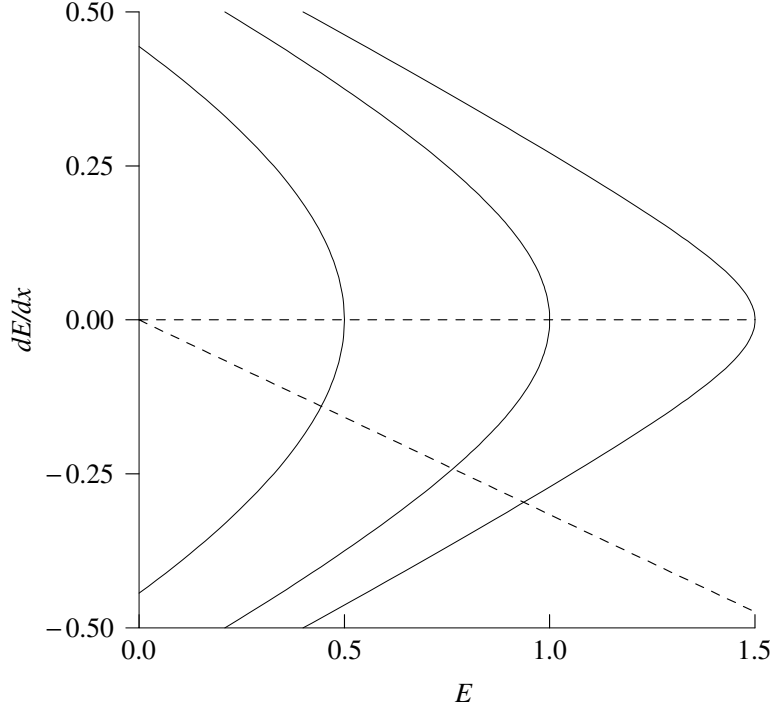


Figure 6. Phase portrait of the solution of the boundary value problem on the upper branch  $g_+(E)$ , with parameter values  $K_A = 1.0$ ,  $V_A = 1.0$ ,  $A_0 = 0.05$ ,  $\delta = 0.1$ ,  $\rho = 0.3$ ,  $k_A = 0.2$ , and  $k_E = \alpha^2 = 0.1$ . Dashed lines are the curves on which  $E_x = -\alpha E$  and  $E_x = 0$ .

$A_{mx} < A_{mn} < A_0$ , which are local maximum and local minimum, respectively, for the function  $E(A)$ , and that  $E_{mx} = E(A_{mx})$ . The value  $E_{mn} = E(A_{mn})$  may be positive or negative, however, it is required that  $E_{mn} < E_{mx}$ .

Now we invert the function  $E(A)$  by reversing the axes, and note that the inverse function has three branches, a lower, middle and upper branch. For each of these we find the quantity

$$g(E) = \frac{\delta}{1-\rho} (A^{-1}(E) - E) - k_E E, \quad (30)$$

where

$$A^{-1}(E) - \frac{\rho}{\delta} F(A^{-1}(E)) = E. \quad (31)$$

Of necessity,  $g(E)$  has three branches, which we denote as  $g_-(E)$ ,  $g_0(E)$ , and  $g_+(E)$ , shown in Fig. 5. These are defined on the three subintervals  $0 \leq E \leq E_{mx}$  (for  $g_-(E)$ ),  $E_{mn} < E < E_{mx}$  (for  $g_0(E)$ ), and  $E_{mx} < E < E_0$  (for  $g_+(E)$ ), and  $g_+(E_0) = 0$ . Where they are comparable,  $g_-(E) < g_0(E) < g_+(E)$ .

The final restriction placed on the parameters is that we require  $k_E$  to be small enough so that  $g_-(E) > 0$  on the interval  $0 \leq E \leq E_{mx}$ .

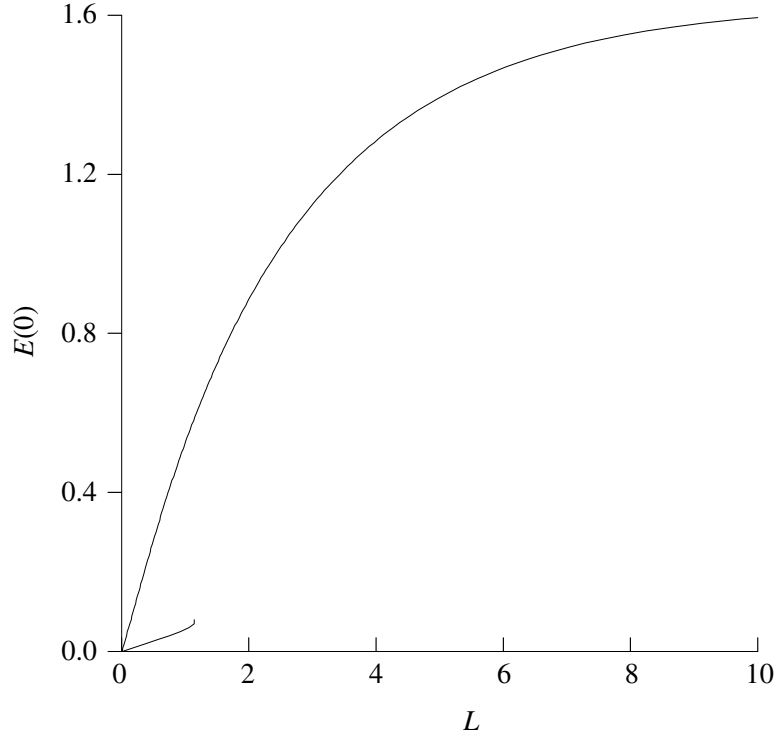


Figure 7. Steady solution branches with  $E(0)$  plotted as a function of  $L$  shown for parameter values  $K_A = 1.0$ ,  $V_A = 1.0$ ,  $A_0 = 0.05$ ,  $\delta = 0.1$ ,  $\rho = 0.3$ ,  $k_A = 0.2$ , and  $k_E = \alpha^2 = 0.1$ .

Now we look for solutions of the ordinary differential equation

$$E_{xx} + g(E) = 0 \quad (32)$$

on the interval  $0 < x < L$  and subject to boundary conditions  $E_x(0) = 0$  and  $E_x(L) = -\alpha E(L)$  where  $\alpha > 0$ . The easiest way to demonstrate the existence of such solutions is in the  $E - E_x$  phase plane, depicted in Fig. 6. In this plane, the boundary conditions are depicted as two straight lines  $E_x = 0$  and  $E_x = -\alpha E$ . In Fig. 6, trajectories are shown for the function  $g_+(E)$  although the trajectories for  $g_-(E)$  are qualitatively identical.

We use the function  $g_-(E)$  to construct the first solution branch. In fact, for any  $E_-$  with  $E_- < E_{m,x}$ , the trajectories with  $E \leq E_-$  and

$$\frac{1}{2}E_x^2 - \int_E^{E_-} g_-(E)dE = 0 \quad (33)$$

work. It follows that for each  $E_-$  with  $0 < E_- < E_{m,x}$  there is a corresponding value of  $L$ , say  $L = L_-(E_-)$ , for which this solution exists. Furthermore, since

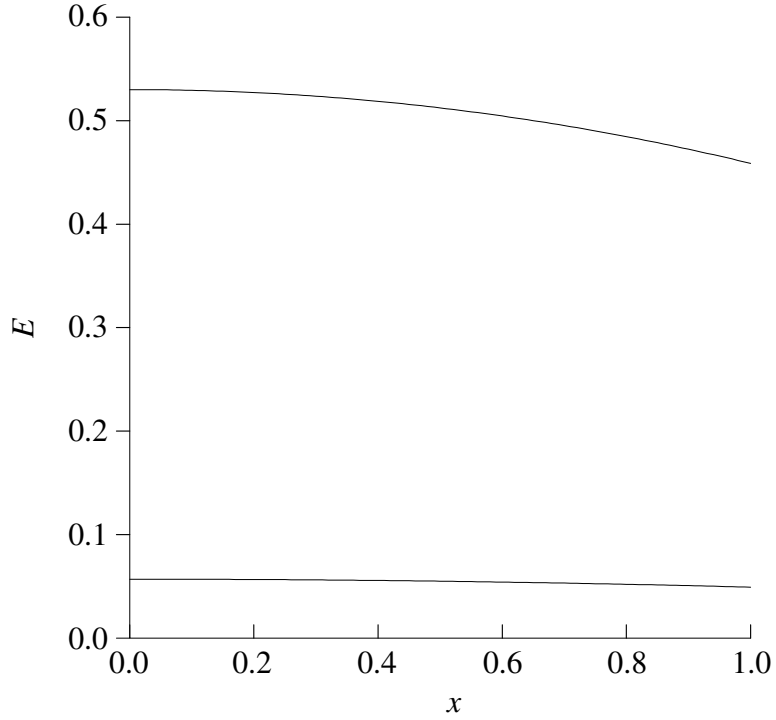


Figure 8. Steady solution profiles  $E(x)$  plotted as a function of  $x$  on the interval  $0 < x < L = 1.0$  for which  $E(0) = 0.057$  on the lower branch and  $E(0) = 0.53$  on the upper branch, shown for parameter values  $K_A = 1.0$ ,  $V_A = 1.0$ ,  $A_0 = 0.05$ ,  $\delta = 0.1$ ,  $\rho = 0.3$ ,  $k_A = 0.2$ , and  $k_E = \alpha^2 = 0.1$ .

$g_-(E)$  is positive and bounded away from 0,  $L_-(E_-)$  remains bounded on its range of existence. In other words, there is a number, say  $L_*$ , which bounds  $L_-(E_-)$  above,  $L_* \leq L_-(E_-)$ . This solution branch is depicted by the smaller of the two curves in Fig. 7 with  $E(0)$  shown plotted as a function of  $L$ . This solution branch terminates at  $L_*$  since the trajectories for the phase portrait can only be defined on the range of definition of  $g_-(E)$ . A typical solution profile is depicted by the smaller of the two curves in Fig. 8.

The second branch of solutions of interest uses  $g_+(E)$  on the interval  $\max\{E_{mn}, 0\} < E < E_0$ . The phase portrait trajectories are solutions of

$$\frac{1}{2}E_x^2 - \int_E^{E_+} g_+(E)dE = 0 \quad (34)$$

provided  $E \leq E_+ \leq E_0$ . Now, however, since  $g_+(E_0) = 0$ , the point  $E = E_0$ ,  $E_x = 0$  is a saddle point in the phase plane. Thus, the trajectory emanating from this point corresponds to  $L = \infty$ . It follows that there is a second solution branch which can be represented as  $L = L_+(E_+)$  with  $L_1 < L < \infty$ . Furthermore, if  $E_{mn} < 0$ , then  $L_1 = 0$ . This solution branch is depicted by the larger of the two

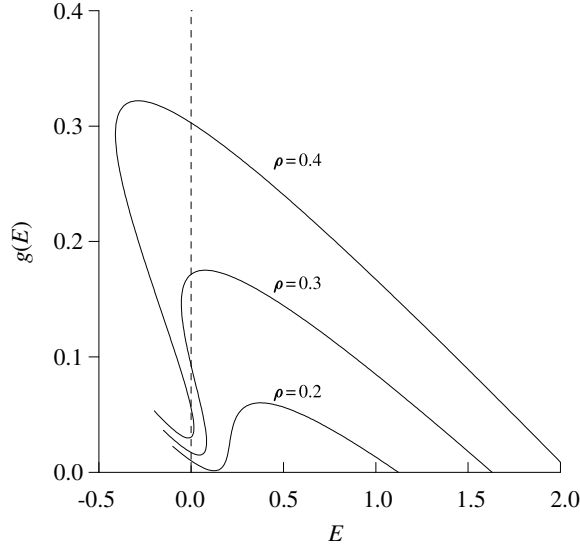


Figure 9. Plot of the 'function'  $g(E) = \frac{\delta}{1-\rho}(A^{-1}(E) - E) - k_e E$  for  $K_A = 1.0$ ,  $V_A = 1.0$ ,  $A_0 = 0.05$ ,  $\delta = 0.1$ ,  $k_A = 0.2$ ,  $k_E = 0.1$ , and three different values of  $\rho$ .

curves in Fig. 7 with  $E(0)$  shown plotted as a function of  $L$ . This solution branch extends to  $L = \infty$  since the trajectory that contains the point  $E_0$  is the unstable manifold of a saddle point. A typical solution profile is depicted by the larger of the two curves in Fig. 8.

Quorum sensing in a spatially distributed system can now be described. If the density  $\rho$  is too small or the size  $L$  is small, the small steady solution is attained. However, if the density is sufficiently large, then as the colony size  $L$  grows, the small steady solution ceases to exist, and the solution switches to the large steady solution. Note that this switch fails if  $k_E$  is too large, since then the curve  $g_-(E)$  is not strictly positive, and therefore the small solution branch exists for all positive  $L$ .

A second way to describe quorum sensing is as a function of density  $\rho$ . We suppose that there is a colony of a fixed size  $L$  that is growing so that the density  $\rho$  is slowly increasing.

It is clear from Fig. 9 that for  $\rho$  sufficiently small there is only the single solution branch  $g_-(E)$ , while for  $\rho$  sufficiently large the only branch defined for positive  $E$  is the  $g_+$  branch. In other words, if  $\delta$  is sufficiently small, there is a value of  $\rho < 1$  above which  $E_{mx} < 0$ . However, if  $E_{mx} < 0$ , the lower branch of solutions fails to exist. Thus, for any fixed  $L$ , there is a value of  $\rho$  above which the lower solution fails to exist. At this value of  $\rho$ , the solution must switch to the upper branch, if stable, thereby dramatically increasing the production of autoinducer.

We have numerically computed a branch of steady-state solutions of (23) and (24) as a function of the density  $\rho$  for fixed domain size  $L$ . These results are shown in Fig. 10. We have found that the upper and lower branches are stable while the

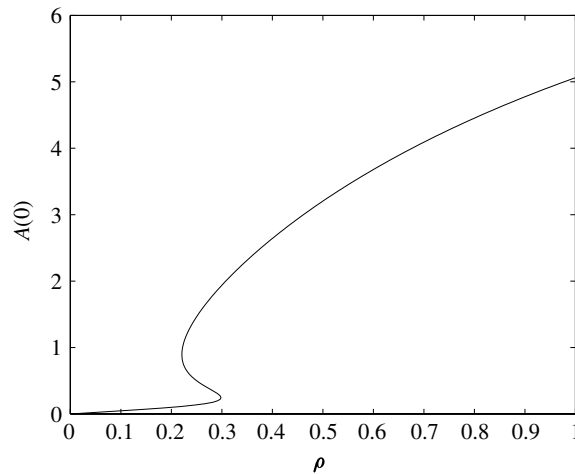


Figure 10. Plot of the bifurcation diagram for the steady states of (23) as a function of the cell density  $\rho$  with  $L$  fixed at  $L = 2$ . The parameter values are  $K_A = 1.0$ ,  $V_A = 1.0$ ,  $A_0 = 0.05$ ,  $\delta = 0.1$ ,  $k_A = 0.2$ ,  $k_E = 0.1$ ,  $\rho = 0.3$ ,  $\alpha = 1.0$ , and  $L = 2.0$ .

middle branch is unstable. As the cell density increases, the production of the autoinducer increases slowly until a critical value of the density is reached. At this point there is a large increase in autoinducer production. Once on the upper branch, the population maintains a high rate of autoinducer production even if the cell density decreases. However, if the cell density falls below the value at the knee on the upper branch, production falls back to a nominal rate.

It has been shown (Davies *et al.*, 1998) that autoinducers can increase polymer production. With increased polymer the cell density would decrease. Thus we see that hysteresis assures that the switch to high autoinducer production is not easily reversed by a decrease in cell density due to an increase in polymer production. It is also easy to speculate that once the cell density becomes low enough that the autoinducer is reset to basal levels, the genes responsible for polymer production are turned off. If there is too much polymer, the diffusion of vital nutrients to the population could be hindered.

In summary, quorum sensing can be accomplished by increasing the density of a colony of fixed size, or by increasing the size of a colony of large enough density.

In the next section, stability results are discussed.

#### 4. STABILITY RESULTS

The stability of the steady state can be determined by numerical simulations of the system or by linearization (Weinberger, 1983).

The following proposition implies that the large and small amplitude steady-state solutions to our system are stable provided that on the range of the steady solution

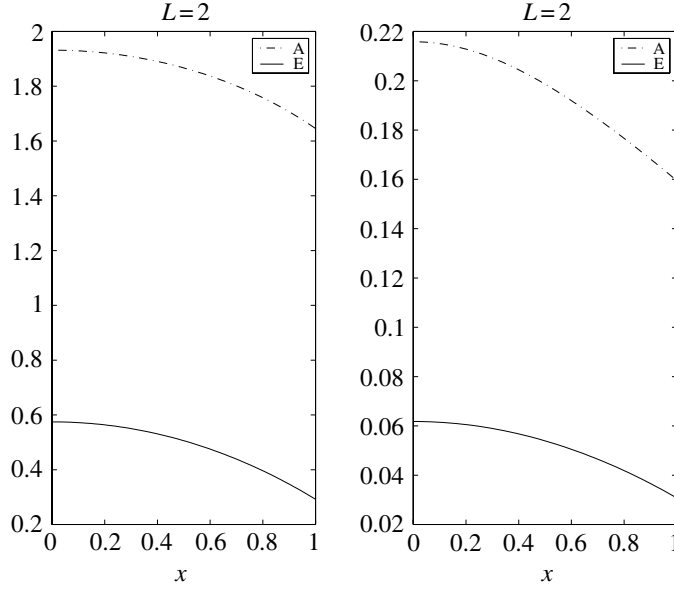


Figure 11. Plot of two different solutions of (23), (24) at  $t = 200$ . The parameter values are  $K_A = 1.0$ ,  $V_A = 1.0$ ,  $A_0 = 0.05$ ,  $\delta = 0.1$ ,  $k_A = 0.2$ ,  $k_E = 0.1$ ,  $\rho = 0.3$ ,  $\alpha = 1.0$ , and  $L = 2.0$ .

$(A_0, E_0)$ ,  $g'(E_0(x)) < 0$ . We show this by constructing time-independent upper and lower solutions that are arbitrarily close to the steady-state solutions.

The system (23), (24) is a cooperative system (quasi-monotone), the right-hand side of (23) is an increasing function of  $E$  and the right-hand side of (24) is increasing in  $A$ . This allows one the following Comparison Principle.

DEFINITION 1. The pair  $(\bar{A}, \bar{E})$  is an upper solution pair for the system (23), (26) if and only if

$$\bar{A}_t \geq F(\bar{A}) + \frac{\delta}{\rho}(\bar{E} - \bar{A}) \tag{35}$$

$$\bar{E}_t \geq \frac{\partial^2 \bar{E}}{\partial x^2} + \frac{\delta}{1 - \rho}(\bar{A} - \bar{E}) - k_E \bar{E} \tag{36}$$

$$\bar{E}_x(L) + \alpha \bar{E}(L) \geq 0 \tag{37}$$

$$\bar{E}_x(0) \leq 0. \tag{38}$$

The pair  $(\underline{A}, \underline{E})$  is a lower solution pair if it satisfies the above with each inequality reversed.

**THEOREM 1 (COMPARISON PRINCIPLE).** Let  $(\bar{A}(x), \bar{E}(x))$  be a  $t$ -independent upper solution pair for the system (23)–(26) and let  $(A(x, t), E(x, t))$  be the solution to the system with the initial data  $(\bar{A}(x), \bar{E}(x))$ . Then  $A$  and  $E$  are nonincreasing functions of  $t$  and approach the largest steady-state solution  $(A^*(x), E^*(x))$

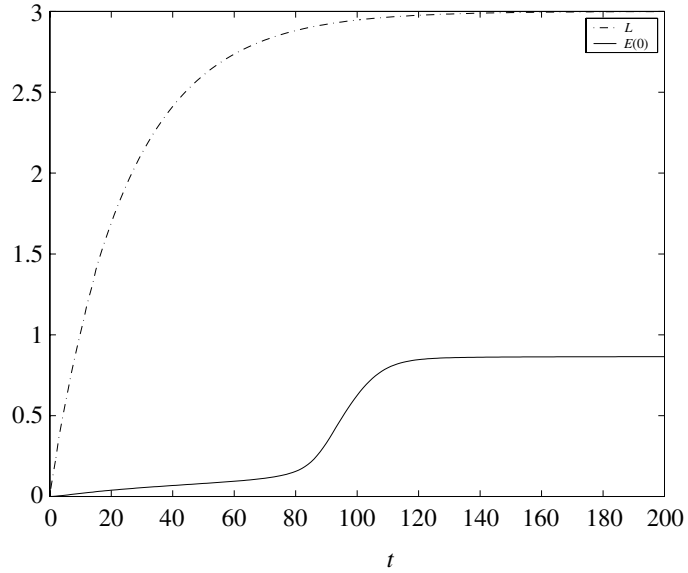


Figure 12. Plot of  $L(t)$  and  $E(0, t)$  starting from constant initial data  $E(x, 0) = 0.0$ ,  $A(x, 0) = 0.0$ ,  $L(0) = 0.01$ . The parameter values are  $K_A = 1.0$ ,  $V_A = 1.0$ ,  $A_0 = 0.05$ ,  $\delta = 0.1$ ,  $k_A = 0.2$ ,  $k_E = 0.1$ ,  $\rho = 0.3$ ,  $\alpha = 1.0$ , and  $L = 2.0$ .

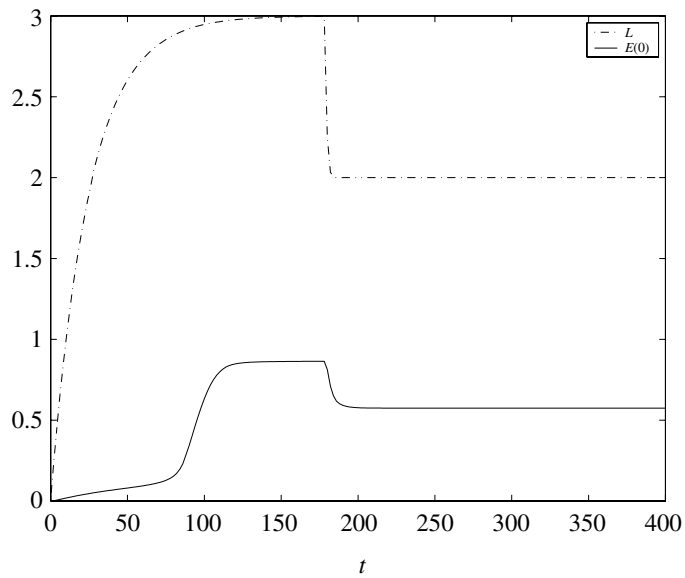


Figure 13. Plot of  $L(t)$  and  $E(0, t)$  starting from constant initial data  $E(x, 0) = 0.0$ ,  $A(x, 0) = 0.0$ ,  $L(0) = 0.01$ . The parameter values are  $K_A = 1.0$ ,  $V_A = 1.0$ ,  $A_0 = 0.05$ ,  $\delta = 0.1$ ,  $k_A = 0.2$ ,  $k_E = 0.1$ ,  $\rho = 0.3$ ,  $\alpha = 1.0$ , and  $L = 2.0$ .

that satisfies  $A^*(x) \leq \bar{A}(x)$  and  $E^*(x) \leq \bar{E}(x)$ . Similarly, let  $(\underline{A}(x), \underline{E}(x))$  be a lower solution pair to the system and  $(A(x, t), E(x, t))$  a solution with  $(\underline{A}(x), \underline{E}(x))$  as initial data. Then  $(A(x, t), E(x, t))$  are nondecreasing in  $t$  and tend to the smallest stationary solution,  $(A_*(x), E_*(x))$  that lies above  $(\underline{A}(x), \underline{E}(x))$ .

Let  $(A_0(x), E_0(x))$  be a steady-state solution of (23)–(26) and let  $\epsilon > 0$  be fixed but arbitrary. Consider

$$\hat{E}(x) = E_0(x) + \epsilon \quad (39)$$

$$\hat{A}(x) = A^{-1}(E_0(x) + \epsilon). \quad (40)$$

We show that  $(\hat{A}, \hat{E})$  is an upper solution pair provided certain conditions are satisfied. First, we assume that our steady solution lies either on the upper branch of  $A^{-1}$  or the lower branch. It is clear from Fig. 4 that  $A^{-1}$  is an increasing function of  $E$  on these two branches, thus

$$\hat{A}(x)q = A^{-1}(E_0(x) + \epsilon) \geq A^{-1}(E_0(x)) = A_0(x)$$

if  $\epsilon > 0$  is sufficiently small. It follows that  $(\hat{A}, \hat{E})$  satisfies (35). It is also clear that the boundary inequalities (37), (38) are satisfied.

Now consider inequality (36). If we assume that  $g$  is nonincreasing on the range of  $E_0$ , then for small enough  $\epsilon$  we obtain

$$\hat{E}_{xx} + g(\hat{E}) = E_{0,xx} + g(E_0 + \epsilon) \quad (41)$$

$$\leq E_{0,xx} + g(E_0) = 0 \quad (42)$$

and we see that (36) is satisfied. The following result follows from Theorem 1.

**PROPOSITION 1.** *Let  $(A_0, E_0)$  be a steady-state solution which lies on the upper or lower branch of  $g$ ,  $g_{\pm}$ . If on the range of  $E_0(x)$ ,  $g$  is nonincreasing, then for  $\epsilon$  sufficiently small and positive  $(A_0(x) + \epsilon, E_0(x) + \epsilon)$  is an upper solution pair and  $(A_0(x) - \epsilon, E_0(x) - \epsilon)$  is a lower solution pair. Furthermore, in this case  $(A_0, E_0)$  is a stable solution of (23)–(26).*

While in general we cannot verify that  $g_{\pm}$  are decreasing functions for all parameter values, it is clear from Fig. 9 that this is the case for  $g_+(E)$  for large enough values of  $\rho$ , and for  $g_-(E)$  for small enough values of  $L$ .

There are also steady solutions that correspond to the middle branch of  $g$ ,  $g_0$ . We can show that these solutions are unstable.

**PROPOSITION 2.** *Steady-state solutions  $(A_0(x), E_0(x))$  for which  $E'(A_0(x)) < 0$  are linearly unstable.*

To prove this, consider the linearization of (23), (24) about a steady solution  $(A_0, E_0)$

$$a_t = F'[A_0(x)]a + \frac{\delta}{\rho}(e - a), \quad (43)$$

$$e_t = e_{xx} + \frac{\delta}{1 - \rho}(a - e) - k_E e. \quad (44)$$

Let  $\alpha(x) = F'[A_0(x)] - \frac{\delta}{\rho}$ , and note that  $\alpha(x) = -\frac{\rho}{\delta}E'[A_0(x)]$ , which is positive on the middle branch. Suppose that  $(a, e)$  is a solution of (43), (44) with  $(a(x, 0), e(x, 0)) = (a_0(x), e_0(x))$  and such that  $e(x, t)$  remains bounded for all  $t \geq 0$ , say  $|e(x, t)| \leq M$ . Then from (43) we see that

$$a_t \geq \alpha(x)a - M\frac{\delta}{\rho}$$

which implies that

$$a(x, t) \geq \exp(\alpha(x)t)a_0(0) + \frac{M\delta}{\rho\alpha(x)}(1 - \exp(\alpha(x)t))$$

so that  $a(x, t)$  cannot remain bounded for all  $t > 0$  if we start with positive initial data, which implies instability. If  $e(x, t)$  is unbounded for  $t > 0$  starting from arbitrarily small initial data, then clearly the steady solution is linearly unstable.

## 5. NUMERICAL SIMULATIONS

In this section we report on numerical simulations which illustrate the stability results of the previous section. We also indicate how these results may be applicable to biofilms.

We take  $\alpha = 1$  and scale the  $x$  interval to have unit length. In Fig. 11 are displayed the two stable steady states that exist when  $L = 2$ . One is an order of magnitude larger than the other. The small solution was generated from the constant initial data  $A(x, 0) = 0.0$  and  $E(x, 0) = 0$ . The larger solution was also generated from constant initial data,  $A(x, 0) = 1.0$  and  $E(x, 0) = 1.0$ . Both solutions are shown at time  $t = 200$ . At this time the time derivatives of both  $A$  and  $E$  are less than  $10^{-10}$  so we take these to be steady states.

One can model a growing population by adding dynamics for the domain length  $L$ . Here we set

$$\frac{dL}{dt} = \kappa(L_f - L) \quad (45)$$

where  $\kappa = 0.04$  and  $L_f = 3$ .

The time series of a solution of (23), (24) and (45) with constant initial data is shown in Fig. 12. Here we display the length of the interval  $L$  and the value of the extracellular autoinducer at  $x = 0$ ,  $E(0, t)$  as functions of time. From other numerical calculations we know that the small amplitude solution does not exist at  $L = 2.2$ . We see that after a lag the solution of the evolution equation approaches the large amplitude steady solution that exists at  $L = 3$ .

To demonstrate the hysteresis indicated in Fig. 7, we use the same dynamics for  $L$  as above in a second run until  $t = 180$  whereupon we set  $L = 2$ . This could be thought of as a major detachment event whereby the biofilm thickness is suddenly reset to two thirds of its asymptotic thickness. The time series of such a solution is shown in Fig. 13. We see that upon reset, the autoinducer concentration remains high. The hysteresis assures that the switch to high autoinducer production is not easily reversed. This is very important for a biofilm since these populations are often subjected to major detachment and sluffing events whereby there are large and sudden decreases in population size.

## 6. DISCUSSION

We have presented a simple model of quorum sensing using autoinduction that is based on the known biochemistry of *P. aeruginosa*. Using this model we demonstrate that quorum sensing works because the rate of elimination of autoinducer depends on the colony size and density. Thus, the autoinducer production switches to its high state when the elimination of autoinducer from the extracellular space is decreased.

This biochemical switch is hysteretic so that autoinducer production switches on at different (higher) levels than it switches off. This hysteresis is possibly important in the regulation of the production of exopolysaccharide, which tends to decrease bacterial density. The hysteresis predicted by this model investigation has not been verified experimentally.

## ACKNOWLEDGEMENTS

JDD was supported in part by NSF grant DMS-9805701. JPK was supported in part by NSF grant DMS-99700876.

## REFERENCES

- Anderson, J. B., C. Sternberg, L. K. Poulsen, M. Givskov and S. Molin (1998). New unstable variants of green fluorescent protein for studies of transient gene expression in bacteria. *Appl. Environ. Microbiol.* **64**, 2240–2246.
- Chalfie, M., Y. Tu, G. Euskirchen, W. W. Ward and D. C. Prasher (1994). Green fluorescent protein as a marker for gene expression. *Science* **263**, 802–805.

Editor:  
position of reference Van  
Delden and  
Iglewski(1998) OK?  
(Alphabetical order)

- Characklis, W. G. and K. C. Marshall (1990). *Biofilms*, New York: John Wiley & Sons, Inc.
- Author: Davies, D. G., M. R. Parsek, J. P. Pearson, B. H. Iglewski, J. W. Costerton and E. P. Greenberg (1998). The involvement of cell-to-cell signals in the development of bacterial biofilm. *Science*.
- Please supply more details of reference Davies *et al.* (1998)
- Author: Van Delden, C. and B. H. Iglewski (1998). Cell-to-cell signaling and *Pseudomonas aeruginosa* infections. *Emerging Infect. Dis.* **4**(4).
- Please supply more details of reference Van Delden *et al.* (1998);
- Editor: Ehrenberg, M. and A. Sverredal (1995). A model for copy number control of the plasmid R1. *J. Mol. Biol.* **246**, 472–485.
- Issue number OK?
- Fuqua, C., S. C. Winans and E. P. Greenberg (1996). Census and concensus in bacterial ecosystems: The luxR-luxI family of quorum-sensing transcriptional regulators. *Annu. Rev. Microbiol.* **50**, 727–751.
- Author: Govan, J. R. and V. Deretic (1996). Microbial pathogenesis in cystic fibrosis: mucoid *pseudomonas aeruginosa* and *Burkholderia cepacia*. *Microbiol. Rev.*
- Please supply more details of reference Govan and Deretic (1996)
- James, S., P. Nilsson, G. James, S. Kjelleberg and T. Fagerström (2000). Luminescence control in the marine bacterium *Vibrio fischeri*: An analysis of the dynamics of lux regulation. *J. Mol. Biol.* **296**, 1127–1137.
- Pearson, J. P., C. Van Delden and B. H. Iglewski (1999). Active efflux and diffusion are involved in transport of *Pseudomonas aeruginosa* cell-to-cell signals. *J. Bacteriol.* **181**(4), 1203–1210.
- Editor: Ward, J. P., J. R. King and A. J. Koerber (2000). Mathematical modelling of quorum sensing in bacteria. Preprint.
- Issue number OK?
- Weinberger, H. F. (1983). A simple system with a continuum of stable inhomogeneous steady states, in *Nonlinear Partial Differential Equations in Applied Science (Tokyo, 1982)*, Amsterdam: North-Holland, pp. 345–359.

Received 16 January 2000 and accepted 3 September 2000